

# A Molecular Density Functional Theory of aqueous electrolytic solution.

Guillaume Jeanmairet

*Sorbonne Université, CNRS, Physico-Chimie des Électrolytes et Nanosystèmes Interfaciaux,  
PHENIX, F-75005 Paris, France and  
Réseau sur le Stockage Electrochimique de l'Énergie (RS2E),  
FR CNRS 3459, 80039 Amiens Cedex, France*

Luc Belloni

*LIONS, NIMBE, CEA, CNRS, Université Paris-Saclay, 91191 Gif-sur-Yvette, France*

Daniel Borgis

*PASTEUR, Département de chimie,  
École normale supérieure, PSL University,  
Sorbonne Université, CNRS, 75005 Paris, France and  
Maison de la Simulation, CEA, CNRS, Université Paris-Sud,  
UVSQ, Université Paris-Saclay, 91191 Gif-sur-Yvette, France*

## Abstract

We propose a generalisation of molecular density functional theory to describe inhomogeneous solvent mixture, with the objective of modelling electrolytic solutions. Two electrolytic models are presented, both within the HNC approximation. The first one is a two-components mixture representing a primitive-like model of sodium chloride, where the solvent is described as a dielectric continuum. This popular model has the advantage of simplicity, as the ions densities solely depend on spatial coordinates. Additionally, we develop a realistic three-components electrolyte model, in which water solvent is described by a third density field that depends on both spatial and orientational coordinates. The proposed methodology and its tridimensional implementation (3 spatial coordinates and 3 Euler angles) are validated by comparing the solvation properties of a sodium cation with the predictions of integral equation theory solved in 1D (1 intermolecular distance and 5 Euler angles), showing near-perfect agreement. This methodology enables the study of solvation properties of solutes of arbitrary shapes in electrolytic solutions, as demonstrated with the prototypical N-methylacetamide molecule immersed in both electrolytic solution models.

## I. INTRODUCTION

Electrolytic solutions, i.e solutions containing ions, are present in a wide variety of chemical systems. For instance, ions play a key role in biology, influencing protein stability[1] and protein-protein interactions[2]. Another economically significant application is electrochemical storage, particularly Li-ion batteries and supercapacitors. While Li-ion batteries store energy through Faradaic processes, supercapacitors store charge via ion adsorption at electrode surfaces. The interfacial region, where ion concentrations deviate from equilibrium, is termed the electrical double layer (EDL).

Therefore, in computer simulations of biological objects and electrochemical devices, it is essential to have a realistic description of the electrolyte, especially of the electrostatic interactions. The most accurate strategy is to explicitly describe the constituents of the electrolyte. This is the strategy adopted in molecular simulations such as Monte Carlo and molecular dynamics (MD), which has been successfully employed for the modelling of many biological objects, ranging from proteins[3] to DNA[4], and for supercapacitors[5–7]. However, these approaches become very costly when simulating large systems and/or when long simulation times are required, partly because of the large number of solvent and

electrolyte molecules required to solvate the system.

Following the pioneering work of Gouy, Chapman, and Stern (GCS)[8], there is a long tradition of investigating electrolyte at interface using theoretical approaches rather than simulations. A common strategy is to use implicit solvent models in which the solvent, usually water, is described by a dielectric continuum. In practice, the idea is to define a cavity where lies the solute, for instance a protein. The dielectric constant is assumed to vary from its bulk value outside the cavity towards another small value inside the protein. The value of the dielectric inside the protein[9, 10] and the shape of the boundary[11, 12] influences the predictions, which explain why several choices have been proposed for both. The electrostatic potential can then be obtained by solving the Poisson equation. It is also possible to include ions at the same level of description, whose density is assumed to follow Boltzmann statistics. The solution of the Poisson equation for the electrostatic potential coupled with the Boltzmann statistics for ions give rise to the popular Poisson-Boltzmann (PB) model of electrolytes.

This model suffers from several limitations, in particular the ions are assumed to be point charges. The absence of size effects can lead to abnormally large ionic concentrations close to charged solutes. Another limitation is that ion-solvent and ion-ion correlations are neglected. Several modification of the Poisson-Boltzmann model have been proposed to address these flaws[13–15].

There is another strategy that avoids the tedious sampling of the solvent degrees of freedom while maintaining a microscopic description of the solvent, that is to use liquid state theories. The main strategy is to use integral equation theory (IET) in which the components of the solvent are no longer described by a set of discrete particles. Instead, the average probability to find the solvent components at a given position with respect to the solute is contained into some distribution functions. By solving a coupled set of integral equations, namely the exact Ornstein Zernike (OZ) equation, associated with an approximated closure relation, it is possible to have access to the solvent structure surrounding the solute.

However, solving the OZ equation for molecular solvents, such as water, and complex 3D solutes, as encountered in biology, can be difficult due to the high number of dimensions. This is why further approximations were proposed, a popular one being the reference interaction site model (RISM)[16, 17] which approximates the molecular solvent distribution by distributions of atomic sites. This approach, and its 3D-RISM version, has been widely

employed to study small molecular solutes, either described with classical force fields or quantum mechanics[18–22].

IET has also been adopted to simulate proteins[23–26] and DNA[27, 28]. Despite its success, the 3D-RISM theory is not physically well-grounded, in particular, the assumption that the molecular direct correlation function can be decomposed as a sum of site-site correlation function[29], which is at the core of the theory, is not valid and relies on a crude approximation of the intramolecular correlations.

Classical density functional theory (cDFT) is a functional formulation which is strictly equivalent to IET. The principles of cDFT are the following[30, 31]: i) There exists a unique functional of the particle densities. ii) This functional is equal to the system’s grand potential at its minimum which iii) is reached for the equilibrium particle densities. Therefore, structural and thermodynamic properties can be obtained through functional minimisation rather than by solving integral equations, these latter expressing that the gradient of the functional is zero.

In cDFT, the ionic components of the electrolyte are modelled by their spatially dependant density fields,  $n_+$  and  $n_-$  with the possibility to explicitly account for the solvent with a third density field,  $n_s$ . When a perturbation is present, the particles densities become inhomogeneous. Due to this computational efficiency, cDFT has been used to study electrolytic solution since its early ages[32–34]. Initial attention focused on the primitive model of electrolyte, consisting of oppositely charged hard-sphere in a dielectric continuum.

One of the key achievements of classical DFT is fundamental measure theory (FMT)[34–37] which provides nearly exact results for the hard-sphere fluid. As a result, most recent works use FMT as their starting point to build a functional for electrolytes. In contrast, the description of electrostatic correlations is less straightforward, leading to the development of various strategies. The simplest approach is to treat electrostatic correlation at the mean-field level. When only this correlation is considered, the theory is equivalent to Poisson-Boltzmann theory[38]. Incorporating finite-size effects and hard-sphere correlations makes the theory akin to modified Poisson-Boltzmann approaches[39].

To go beyond mean-field, a common strategy is to perform a Taylor expansion of the functional, truncated at second order, around a reference fluid[33, 40, 41]. However, it is known that this quadratic truncation introduces thermodynamic inconsistencies and other electrostatic functionals based on the weighted-density approximation (WDA)[42–44] have

been proposed to correct this defect.

There is currently a growing interest in the development of machine-learning-based functionals (MLF)[45–47], including the development of a MLF for the restricted primitive model[48].

Regarding the description of the solvent, it may be modelled implicitly through a dielectric continuum that screens the interactions[32, 33, 41, 43, 49], or explicitly as an additional species. Here again, due to the quality of FMT, the solvent is often modelled as an hard-sphere[50] or as combination of hard-spheres[51–53], possibly with added charges or dipolar moments[54–56].

In this paper, we introduce a cDFT framework with the objectives of achieving a more realistic description of both the solvent and the solute. To do so, we will show in section II how the molecular density functional theory (MDFT)[57] framework can be extended to multi-components fluids, *i.e* mixtures. The particularities due to the description of charged species, *i.e* ions, and the modifications it implies for numerical implementation of MDFT will be discussed on the particular case of aqueous electrolytic solution. Here, the solution is described as a three-component mixture made of anion, cation and water. The main result of this paper is this functional which describes an electrolytic solution in a molecular solvent. For comparison, a primitive like two-component functional is also presented.

The 3D MDFT implementation is validated by comparison with the reference 1D-IET computation in section III. This validation is done by comparing the prediction of a sodium cation in a 1M NaCl aqueous solution, with the two electrolyte models. Following validation, we showcase the theory’s capability to analyse complex solutes by examining the solvation of an N-Methylacetamide molecule in the same electrolyte solution models. This molecule involves a single peptide bond and is often considered as the simplest realistic model for the peptide group[58].

## II. THEORY

### A. Molecular Density Functional Theory of Mixtures

Let us consider a  $N$ -component mixture of molecular species. Each molecule is assumed to be rigid such as the knowledge of the position  $\mathbf{r}$  of its center of mass (COM) and of its

absolute orientation  $\mathbf{\Omega}$  is enough to fully describe its set of coordinates.

The objective is to develop a cDFT, which is most naturally formulated in the Grand Canonical ensemble where  $V$ ,  $T$  and the chemical potentials  $\mu_A$ , of all species  $A$  are fixed. Since the entities are molecular and rigid, their one particle densities depend on the space and angular coordinates, *i.e*

$$\rho_A(\mathbf{r}, \mathbf{\Omega}) = \left\langle \sum_{i \in A} \delta(\mathbf{r} - \mathbf{r}_i) \delta(\mathbf{\Omega} - \mathbf{\Omega}_i) \right\rangle, \quad (1)$$

where  $\rho_A$  is the density of species  $A$ , and the sum runs over each molecule of this species.  $\delta$  denotes the Dirac distribution, and the angle brackets indicate the ensemble average in the Grand Canonical ensemble. The angular dependent density  $\rho_A$  is related to the usual number density  $n_A$  through:

$$n_A(\mathbf{r}) = \int \rho_A(\mathbf{r}, \mathbf{\Omega}) d\mathbf{\Omega}. \quad (2)$$

In the presence of an external perturbation, such as in the vicinity of a solute, the molecular densities become inhomogeneous. Following a derivation similar to Mermin and Evans' [30, 31] pioneering work or using Levy-Lieb constrained search[59, 60], it is possible to prove the existence of a unique functional of the set of solvent densities,  $\Omega[\{\rho_1, \rho_2 \dots \rho_N\}]$ , which reaches its minimum when each density equals its equilibrium value. At this minimum, the functional is equal to the grand-potential. Note that this is a straightforward generalisation of the original one-component cDFT which has already been widely used in the literature, in particular for hard-body fluids[34–37]. The originality of the present work lies in developing functionals capable of describing mixtures of molecular fluids. Following the strategy we adopt for one-solvent MDFT, we work with a new functional which is defined as the difference between the functional of the perturbed fluid and the grand potential of the homogeneous mixture,  $\Omega_0$

$$F = \Omega[\{\rho_1, \rho_2 \dots \rho_N\}] - \Omega_0. \quad (3)$$

As usual[31, 61], the functional is split into the sum of three components

$$F[\{\rho_1, \rho_2 \dots \rho_N\}] = F_{\text{id}}[\{\rho_1, \rho_2 \dots \rho_N\}] + F_{\text{ext}}[\{\rho_1, \rho_2 \dots \rho_N\}] + F_{\text{exc}}[\{\rho_1, \rho_2 \dots \rho_N\}]. \quad (4)$$

The ideal part, which is the first term on the right hand side of equation 4, measures the entropic cost for the system to acquire non-homogeneous densities. In this context, it

corresponds to the functional of a mixture of non-interacting fluids.

$$F_{\text{id}}[\{\rho_1, \rho_2 \dots \rho_N\}] = k_B T \sum_{A=1}^N \iint \left[ \rho_A(\mathbf{r}, \boldsymbol{\Omega}) \ln \left( \frac{\rho_A(\mathbf{r}, \boldsymbol{\Omega})}{\rho_{0A}} \right) - \Delta \rho_A(\mathbf{r}, \boldsymbol{\Omega}) \right] d\mathbf{r} d\boldsymbol{\Omega} \quad (5)$$

where the sum runs over the constituents of the mixture and  $\Delta \rho_A = \rho_A - \rho_{0A}$  is the excess density of A with respect to the homogeneous density  $\rho_{0A}$ . The second term is due to the interaction with the external field

$$F_{\text{ext}}[\{\rho_1, \rho_2 \dots \rho_N\}] = \sum_{A=1}^N \iint \rho_A(\mathbf{r}, \boldsymbol{\Omega}) V_{\text{ext}}^A(\mathbf{r}, \boldsymbol{\Omega}) d\mathbf{r} d\boldsymbol{\Omega} \quad (6)$$

where  $V_{\text{ext}}^A$  are external potentials describing the interactions between the solute and the different components of the mixture. In this paper, as in most of our work, the external potentials are parametrised with classical force fields composed of point charges and Lennard-Jones sites. As an alternative, we recently proposed a QM/MDFT framework where the electrostatic part of the external potential is derived from the electronic density, computed using a quantum mechanics description of the solute[60, 62–64].

The last term of equation 4 is the excess term, which arises from the interactions between the particles of the solution. It is possible to perform a systematic expansion of this functional around the homogeneous densities.

$$F_{\text{exc}}[\{\rho_1, \rho_2 \dots \rho_N\}] = -\frac{1}{2} k_B T \sum_{A=1}^N \sum_{B=1}^N \iint [\Delta \rho_A(\mathbf{r}_1, \boldsymbol{\Omega}_1) c_{AB}(\|\mathbf{r}_1 - \mathbf{r}_2\|, \boldsymbol{\Omega}_1, \boldsymbol{\Omega}_2) \Delta \rho_B(\mathbf{r}_2, \boldsymbol{\Omega}_2)] d\mathbf{r}_1 d\mathbf{r}_2 d\boldsymbol{\Omega}_1 d\boldsymbol{\Omega}_2 + F_{\text{Bridge}}[\{\rho_1, \rho_2 \dots \rho_N\}]. \quad (7)$$

In equation 7,  $F_{\text{Bridge}}$  is the so-called bridge term, which contains all terms of order higher than 2 in  $\Delta \rho$ . We have previously worked on several model of bridge functional for pure solvent[65–69], but their transferability to mixture should be studied carefully. Therefore, the bridge term of equation 7 will be omitted in this paper. This corresponds to the solute-solvent HNC approximation in IET language. The second order term involves the  $c_{AB}$  direct correlation functions (dcf) between species A and species B in the homogenous (unperturbed) mixture. The dcf are functions of the relative position and orientations 1, 2 (one distance and five Euler angles).

The dcf can be obtained by solving the molecular Ornstein Zernike equation for the homogeneous mixture at a given temperature and bulk density and are inputs of the present theory.

The exact dcf are obtained using Monte-Carlo data at short distances and complemented with the hypernetted chain closure, which is known to be valid at long distances[70, 71].

Minimisation of equation 4 leads to the following HNC integral equations

$$\rho_A(\mathbf{r}, \mathbf{\Omega}) = \rho_{0A} \exp[-\beta V_{\text{ext}}^A(\mathbf{r}, \mathbf{\Omega}) + \gamma_A(\mathbf{r}, \mathbf{\Omega})]. \quad (8)$$

The indirect solute-solvent pair correlation function  $\gamma_A$  is given by the Ornstein-Zernike (OZ) solute-solvent equation

$$\gamma_A(\mathbf{r}, \mathbf{\Omega}) = \sum_{B=1}^N \iint c_{AB}(\|\mathbf{r} - \mathbf{r}_2\|, \mathbf{\Omega}, \mathbf{\Omega}_2) \Delta \rho_B(\mathbf{r}_2, \mathbf{\Omega}_2) d\mathbf{r}_2 d\mathbf{\Omega}_2. \quad (9)$$

The excess functional of equation 7 and the integral equation 9 involve convolution products.

For molecular solvent, such as water, the angular convolution calculation benefits from the use of an expansion onto a basis of generalized spherical harmonics (GSH)[72, 73]. In Fourier space and in the local intermolecular frame, the integral equation 9 becomes a product between different projections, characterised by three indices for the solute-solvent density distributions, and five indices for the solvent-solvent dcf:

$$\hat{\gamma}_{A\mu;\chi}^m(\mathbf{k}) = \sum_{B=1}^N \sum_{n,\nu} (-1)^{\chi+\nu} \hat{c}_{AB\mu\nu;\chi}^{mn}(k) \Delta \hat{\rho}_{B-\nu;\chi}^n(\mathbf{k}). \quad (10)$$

Note that the exchange between direct and Fourier spaces is made through Fourier-Hankel transforms of projections defined in the fixed, laboratory frame. The  $\chi$  projections, in the local intermolecular frame, used in equation 10 can be obtained using the standard  $\chi$ -transform of Blum[72, 74, 75]. The angular convolution of equation 9 has thus been replaced by matrix products. Moreover, the different values of  $\chi$  are not mixed; there is one simple matrix equation 10 for each value of  $\chi$ . While, in principle, the basis of GSH is infinite, it is truncated for values of  $m, n \leq m_{\text{max}}$  in practice. More details about the overall procedure to compute  $\gamma_A$  can be found in reference [73]. For monoatomic species, there are no angular degrees of freedom, thus  $m_{\text{max}} = 0$  and the unique projection of the density identifies with the number density:  $\rho_{0;0}^0(\mathbf{r}) = n(\mathbf{r})$ .

The functional of equation 4 is minimised numerically using the following procedure. The densities are computed in a orthorhombic box with periodic boundary conditions. They are discretised on a  $N_x \times N_y \times N_z$  spatial grid. Regarding the orientation in the laboratory



frame, the first Euler angle  $\theta$  is discretised using a Gauss-Legendre quadrature while a regular discretisation is used for the remaining angles  $\phi$  and  $\psi$ . The number of angles is related to the choice for  $m_{\max}$ [73].

The cycle starts with a guess for the densities  $\rho_A(\mathbf{r}, \mathbf{\Omega})$ , from which the functional of equation 4 and its gradient at each grid point are computed. We take advantage of the fast Fourier transform (FFT), computed with the FFTW3 package[76] to handle the spatial convolution, while the angular convolution is taken care of through the use of projections on rotational invariants using equation 10 following the procedure described for one component solvent[73]. The quasi-Newton LBFGS optimiser[77] is used to propose a set of new densities  $\rho_A(\mathbf{r}, \mathbf{\Omega})$ . This procedure is iterated until convergence is reached. Note that due to the logarithm in the expression of the ideal functional in equation 5, negative values of the density must be prevented during the optimisation process. This condition is enforced by using auxiliary functions  $\xi_A$  as the minimisation variables. These are related to the density through the relationship

$$\rho_A(\mathbf{r}, \mathbf{\Omega}) = \rho_{0A} \xi_A^2(\mathbf{r}, \mathbf{\Omega}) \quad (11)$$

The presence of charged particles, such as ions, in the solvent mixture requires special treatment. Due to the long-range  $1/r$  Coulombic potential, the ion-ion dcfs  $\hat{c}_{AB}(q)$  diverge as  $-q_A q_B / k^2$  at  $k = 0$ , where  $q_A$  is the charge of species A. These divergences impose that the ionic density profiles must fulfil the electroneutrality condition for the total cell, during the whole optimisation process. In order to avoid numerical divergence, we somewhat artificially impose electroneutrality by using an alternative definition for the density of the 1:1 salt as:

$$n_+(\mathbf{r}) = n_0 V \left( 1 + \lambda - \frac{Q}{n_0 V} \right) \frac{\xi_+^2(\mathbf{r})}{\int \xi_+^2(\mathbf{r}) d\mathbf{r}} \quad (12)$$

$$n_-(\mathbf{r}) = n_0 V (1 + \lambda) \frac{\xi_-^2(\mathbf{r})}{\int \xi_-^2(\mathbf{r}) d\mathbf{r}} \quad (13)$$

where  $Q$  is the total charge of the solute. With this definition, the electroneutrality is fulfilled, as  $\int (n_+(\mathbf{r}) - n_-(\mathbf{r})) d\mathbf{r} + Q = 0$ . The additional variable  $\lambda$  allows the number of ions in the cell to fluctuate.

The present 3D version of MDFT, where the spatial positions of the solvent molecules are described by the  $(x, y, z)$  coordinates of their center of mass, is able to manage multi-site solutes of any complex geometry. As a validation test for the proposed methodology, the

solvation of simple spherical ions which are constituents of the 1:1 electrolyte will be considered below. In that case, the full 3D-methodology is not optimal since obvious symmetry relations reduce the number of independent parameters. For such solutes, it is preferable to use a 1D version, where the density profiles depend on the distance  $r$  between the solute and the solvent COM and on the relative orientation of both particles with respect to the vector joining them. This reduces the number of Euler angles needed to describe the relative orientation between the particles from 5 in the general case to only 2 for spherical solutes. In the same spirit as the treatment of bulk solvent correlations, we have developed a 1D integral equation theory (1D-IET) approach to cope with spherical solute dissolved in a general solvent. 1D solute-solvent correlations are expressed as a function of the distance  $r$  and two Euler angles rather than the 3D position  $\mathbf{r}$  and three Euler angles. It uses the robust integral equation machinery[70, 72, 74, 78] developed for the case of molecular particles since the 1970's to solve integral equation 8. The solute-solvent OZ equation 9 is replaced in practice by the alternate expression:

$$\gamma_A(r, \mathbf{\Omega}) = \sum_{B=1}^N \rho_{0B} \iint h_{AB}(\|r - r_2\|, \mathbf{\Omega}, \mathbf{\Omega}_2) c_B(r_2, \mathbf{\Omega}_2) dr_2 d\mathbf{\Omega}_2. \quad (14)$$

The  $h_{AB}$  functions represents the solvent-solvent total pair correlation function in the bulk, unperturbed, fluid. The solute-solvent direct correlation function,  $c_B$ , is related to the other quantities through

$$\gamma_B = h_B - c_B \quad (15)$$

$$h_B = g_B - 1 = \frac{\rho_B}{\rho_{0B}} - 1. \quad (16)$$

Equations 9 and 14 are strictly equivalent since the  $h_{AB}$  and  $c_{AB}$  functions are themselves linked through the solvent-solvent OZ equations. A cycle in the standard 1D IE resolution starts with a guess for  $\gamma_A$ , which allows to calculate  $g_A$  from the integral equation 8 from which  $c_A = g_A - 1 - \gamma_A$  is deduced. The solute-solvent projections  $c_{A\mu\nu}^{mnl}(r)$  are computed in the laboratory frame ( $m = \mu = 0$  and  $n = l$  for spherical solutes) and transformed into the reciprocal space through 1D Fourier-Hankel transforms. This allows to express the OZ equation 14 as products between projections in the intermediate inter-molecular frame. The final  $\gamma_A$  is obtained through the inverse operations.

It is important to highlight that, contrary to the 3D MDFT implementation, the charged species do not cause any numerical problem here. Indeed, the electroneutrality condition in

species	$\sigma$ (Å)	$\epsilon$ (kJ.mol <sup>-1</sup> )	charge ( $e$ )
water (O/H)	3.165/0.0	0.65/0.0	-0.8476/0.4238
Na <sup>+</sup>	2.583	0.416	1
Cl <sup>-</sup>	4.401	0.416	-1

Table I. Force field parameters for the NaCl aqueous solution

the pure solvent imposes exactly

$$\hat{h}_{++}(0) = \hat{h}_{--}(0) = \hat{h}_{+-}(0) - \frac{1}{n_{+0}}. \quad (17)$$

These strict equalities manage without difficulty the analytically known divergence of the  $\hat{c}_{AB}(q)$  functions at  $k = 0$ . 3D-MDFT and 1D-IET are formally equivalent, except that the 3D-MDFT implementation deals with orthorhombic periodic boundaries while 1D-IET implementation assumes a, non-periodic, infinite medium. The direct comparison of those two numerical approaches will serve as joint validation of both methods.

After this general presentation of MDFT for a  $N$  component mixture of molecular species we will focus on the particular case of 1:1 electrolyte aqueous solution.

## B. Aqueous electrolytic solution

### 1. Three components mixture

We consider here a 1:1 aqueous electrolyte, *i.e* a mixture constituted of water, a cationic species and an anionic species. Without loss of generality, we will focus on 1 M NaCl dissolved in SPC/E water whose force-field parameters are given in table I, the temperature is  $T = 298.15$  K.

In MDFT, each component of the fluid is described by its density. Since Na<sup>+</sup> and Cl<sup>-</sup> are 1 site spherical particles their densities  $n_+(\mathbf{r})$  and  $n_-(\mathbf{r})$  solely depend on spatial coordinates while the water density  $\rho_w(\mathbf{r}, \mathbf{\Omega})$  has an additional angular dependancy. Thus, the

components of the functional of equation 4 take the following expression

$$\begin{aligned}
F_{\text{id}}[n_+, n_-, \rho_w] = & k_B T \int \left( n_+(\mathbf{r}) \ln \left( \frac{n_+(\mathbf{r})}{n_0(\mathbf{r})} \right) - \Delta n_+(\mathbf{r}) \right) d\mathbf{r} \\
& + k_B T \int \left( n_-(\mathbf{r}) \ln \left( \frac{n_-(\mathbf{r})}{n_0(\mathbf{r})} \right) - \Delta n_-(\mathbf{r}) \right) d\mathbf{r} \\
& + k_B T \iint \left[ \rho_w(\mathbf{r}, \mathbf{\Omega}) \ln \left( \frac{\rho_w(\mathbf{r}, \mathbf{\Omega})}{\rho_{0w}} \right) - \Delta \rho_w(\mathbf{r}, \mathbf{\Omega}) \right] d\mathbf{r} d\mathbf{\Omega}
\end{aligned} \tag{18}$$

with  $\rho_{0w} = n_{0w}/(8\pi^2)$  where  $n_{0w} = 0.0326 \text{ \AA}^{-3}$  is the number density of water and  $n_{0+} = n_{0-} = 5.94 \times 10^{-4} \text{ \AA}^{-3}$  are the densities of ions in the bulk mixture. The external part of the functional reads

$$F_{\text{ext}}[n_+, n_-, \rho_w] = \int n_+(\mathbf{r}) V_{\text{ext}}^+(\mathbf{r}) d\mathbf{r} + \int n_-(\mathbf{r}) V_{\text{ext}}^-(\mathbf{r}) d\mathbf{r} + \iint \rho_w(\mathbf{r}, \mathbf{\Omega}) V_{\text{ext}}^w(\mathbf{r}, \mathbf{\Omega}) d\mathbf{r} d\mathbf{\Omega}. \tag{19}$$

Neglecting the bridge functional, the excess term of equation 7 now is

$$\begin{aligned}
F_{\text{exc}}[n_+, n_-, \rho_w] = & -\frac{1}{2} k_B T \sum_{y=+,-} \sum_{x=+,-} \iint \Delta n_x(\mathbf{r}_1) c_{xy}(\|\mathbf{r}_1 - \mathbf{r}_2\|) \Delta n_y(\mathbf{r}_2) d\mathbf{r}_1 d\mathbf{r}_2 \\
& - k_B T \sum_{x=+,-} \iiint \Delta n_x(\mathbf{r}_1) c_{xw}(\|\mathbf{r}_1 - \mathbf{r}_2\|, \mathbf{\Omega}_2) \Delta \rho_w(\mathbf{r}_2, \mathbf{\Omega}_2) d\mathbf{r}_1 d\mathbf{r}_2 d\mathbf{\Omega}_2 \\
& - \frac{1}{2} k_B T \iiint \Delta \rho_w(\mathbf{r}_1, \mathbf{\Omega}_1) c_{ww}(\|\mathbf{r}_1 - \mathbf{r}_2\|, \mathbf{\Omega}_1, \mathbf{\Omega}_2) \Delta \rho_w(\mathbf{r}_2, \mathbf{\Omega}_2) d\mathbf{r}_1 d\mathbf{r}_2 d\mathbf{\Omega}_1 d\mathbf{\Omega}_2.
\end{aligned} \tag{20}$$

The angular convolution is efficiently performed by developing the water-water and water-ions convolution products onto a basis of rotational invariants as in equation 10. Since the ions are spherical the expansion is complete for  $m_{\text{max}} = 0$ , while for water the basis set is infinite and needs to be truncated. Choosing  $m_{\text{max}} = 4$  proves to be sufficient to reach a good enough precision. Thanks to the symmetry of the water molecule, the numbers of independent projections for bulk water-water and ion-water dcf,  $c_{AB\mu\nu;\chi}^{mn}$ , are 250 and 9, respectively. The number of independent projection for the water density,  $\rho_{w\mu;\chi}^m$  is 55. This corresponds to 225 independent angles for the angular grid.

The ion-ion dcf employed in the functional of equation 20 are depicted in figure 1. The water-water, ion-water and water-ion dcf are not shown, but two points are noteworthy. Firstly, the water-water dcf do not exhibit significant changes compared to the pure solvent case. Secondly, the  $\hat{c}_{00,0}^{01}(k)$  projection diverges as  $-4\pi L_B q \mu i / \sqrt{3} k$  at small  $k$  for ion-water pairs, where  $qe$  is the charge of the ion,  $\mu e$  is the dipole moment of water and  $i$  is the

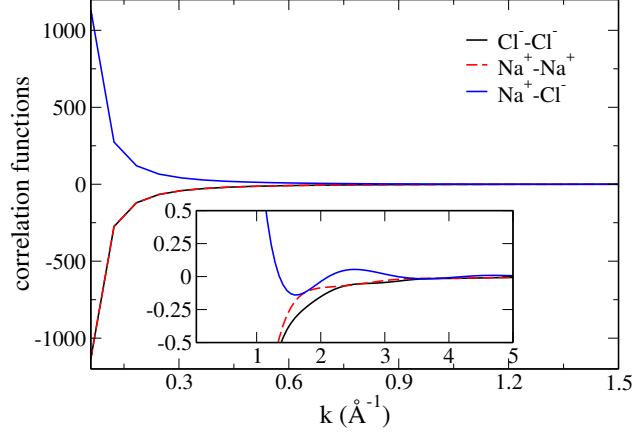


Figure 1. Ion-ion direct correlation functions,  $c_{AB}(k)$ , in the SPC/E NaCl (1M) solution.

imaginary unit. The ion-ion dcf diverge asymptotically as  $-4\pi L_B q q' / k^2$  at small  $k$ , where  $L_B$  is the Bjerrum length, and converge towards 0 at high values of  $k$ . In the intermediate region, each correlations function present some oscillation, as evidenced in the inset of figure 1. This departure from the asymptotic behaviour has two origins; it is a consequence of the finite size effect arising from the Lennard-Jones interaction between ion pairs and of the correlations with water. In the Poisson-Boltzmann case, such oscillation would be absent and the dcf would coincide with their low  $k$  asymptotic behaviour over the entire range of  $k$ .

## 2. Two components mixture: primitive-like model

If we compare the number of projections for the different dcf used to describe the ternary NaCl solution, we notice that only 3 are required to describe the ion-ion terms while 268 involve water. Most of the computational demand originates from the water-water and water-ion interactions. An implicit description of water would reduce drastically the computational cost of the calculation. We thus propose to build a functional for a two-components primitive-like model of 1M NaCl. The Lennard-Jones parameters of the ions remain the same as in table I, but the electrostatic interactions are screened by a factor  $\epsilon_r = 78$ . The expression of the functional is obtained by removing all terms involving water in equations 18-20. It is worth emphasising that the ion-ion dcfs, which are displayed in figure 2, differ from the one used in the ternary mixture. The most obvious feature is their amplitudes being reduced by a factor  $\epsilon_r$  while maintaining an overall similar shape. Noticeable differences

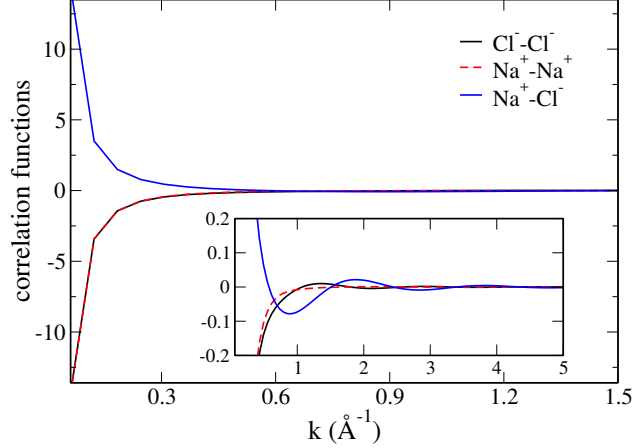


Figure 2. Ion-ion direct correlation functions,  $c_{AB}(k)$ , in the NaCl (1M) primitive-like model.

are also present around  $2\text{--}3 \text{ \AA}^{-1}$ , as evidenced in the insets of figures 1 and 2, because of modified short-range correlations between the ions without water.

### III. RESULTS

#### A. Primitive Model: test particle insertion

As a first test case for our primitive model implementation, we focus on the test particle insertion, i.e the solute is identical to an ion of the solvent mixture. We use cubic box of  $30^3 \text{ \AA}^3$  with a grid resolution of 4 points per  $\text{\AA}$ . We apply the usual type-B correction of Kastenholz *et al*[79] to eliminate contributions arising from periodic replicas of the inserted particle.

In Figure 3, we have compared the radial distribution functions obtained by solving the 1D IET (lines) and by 3D MDFT (symbols). The same direct correlation functions (dcf) were used in both calculations. The agreement is excellent for all three pairs of ions, demonstrating that the 3D MDFT implementation reproduces faithfully the results obtained with the 1D IET resolution.

The solvation free energies, which in this particular case equal the excess chemical potentials of the inserted particles, are reported in Table II. Once again, the agreement between MDFT and IET is nearly perfect.

Again, the main advantage of the 3D MDFT approach over standard IET is that it can

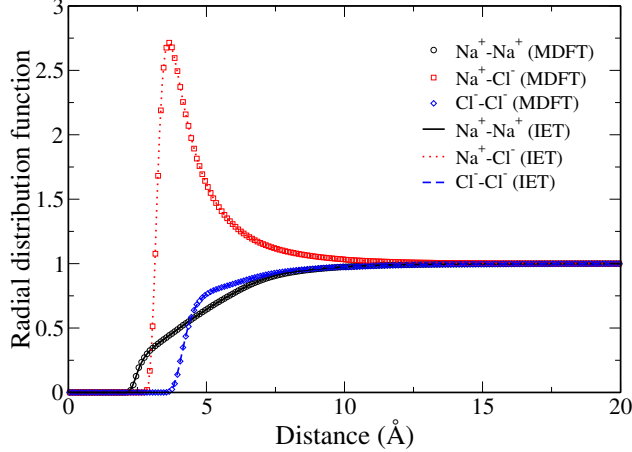


Figure 3. Radial distributions functions between the test ion and ions of the primitive solution determined by using IET (lines) and by MDFT (symbols).

solvent	ion	$\mu_{\text{MDFT}}$ (kJ.mol <sup>-1</sup> )	$\mu_{\text{IET}}$ (kJ.mol <sup>-1</sup> )
primitive	Na <sup>+</sup>	-1.35	-1.36
primitive	Cl <sup>-</sup>	-1.40	-1.41
aqueous	Na <sup>+</sup>	-390.14	-390.37

Table II. Solvation free energies of the inserted ions, as predicted by MDFT and IET. The 2 first lines corresponds to solvation in the primitive model while in the last one water is included explicitly as a third density field

be used to solvate any solutes of arbitrary 3D shape.

To illustrate this functionality, we studied the solvation of the N-methylacetamide (NMA) molecule into the NaCl (1M) primitive-like model. The force-field parameters (charges and Lennard-Jones) are available in SI. In figure 4, we display the densities of chloride and sodium in the plane of the NMA molecule. Our MDFT formulation effectively captures the non trivial arrangement of the ions around the NMA molecule.

There is a cavity around the solute from which the ions are expelled, as evidenced by the dashed areas. This cavity is mostly due to finite size effects caused by the Lennard-Jones interaction, as shown by the larger cavity in the case of the chloride ion, which has a larger Lennard-Jones radius than the sodium ion. At the edge of the cavity begins the first solvation shell of the ions around the NMA molecule.

For the sodium ions, we observe an accumulation around the oxygen atom and a depletion

around the hydrogen atom, while the first solvation shell of chloride shows the opposite trend. These trends arise from the electrostatic interaction: sodium ions are attracted to negatively charged sites and repelled from positively charged ones, whereas chloride ions, bearing a negative charge, exhibit the opposite behaviour. Beyond this first solvation shell, both densities converge toward their bulk value without further significant oscillations. This is corroborated by the radial distribution functions (not reported). The solvent charge density, which is the difference between the sodium density and the chloride density is also reported in figure 4. Here again, the density follows a similar structure: there is a cavity around the solute where the density vanishes due to steric exclusion. This cavity is followed by a first solvation where the charge density reaches non-zero values. Further from the solute, the charge density vanishes again due to electroneutrality of the solution.

Focusing on the solvation shell, there is an excess of sodium ion in the close vicinity of the cavity followed by an excess of chloride ion. This indicates that the overall solvation shell is primarily controlled by steric interactions, i.e. by the difference in cavity sizes for both ions. The role of the electrostatics is secondary, causing a more pronounced excess of sodium ions close to the NMA oxygen which is not followed by an excess of chloride as well as a slight increase in chloride ion excess near the hydrogen atom.

This rationalisation of the solvation pattern in term of LJ and electrostatics contribution has been validated by computing the same quantity for an NMA molecule with zeroed partial charges, with the resulting density maps available in SI. The solvent charge density around the neutralised NMA is similar to the one presented in figure 4, but the modulation of the excess of ions in the vicinity of the O and H atoms of the NMA is no longer present.

The weak influence of the electrostatic interaction is a limitation of the primitive model, because all interactions are scaled by  $1/\epsilon_r$ , including the solute-ions interactions. A more faithful description of the solvent is thus necessary, which is the topic of the next section.

## B. Aqueous electrolyte: test particle insertion

We now turn to the aqueous electrolyte where water is explicitly represented by a density field,  $\rho_w(\mathbf{r}, \mathbf{\Omega})$  which depends on both space coordinates and orientations. Here again, we start by computing the solvation properties around a sodium ion. We use a  $30^3 \text{ \AA}^3$  calculation box with 3 points per  $\text{\AA}$  and  $m_{\max} = 0, 0, 4$  which corresponds to 1, 1 and 225



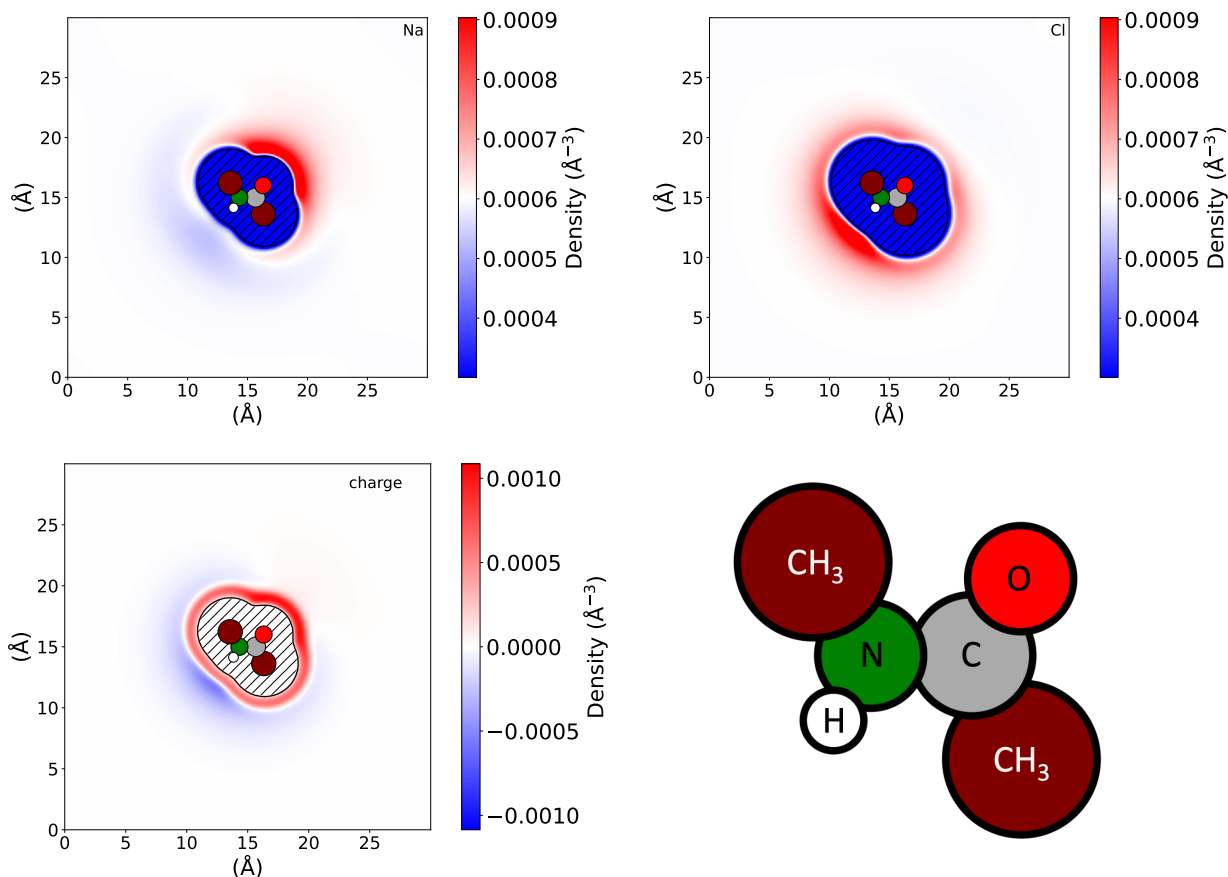


Figure 4. Slices of density in the plane of the NMA molecule. The top panels display the sodium density (left) and the chloride density (right). The bottom panels show the charge density (left), defined as the difference between the sodium density and the chloride density. The right panel explains the colour code for the NMA molecule.

orientations for sodium, chloride and water respectively. We apply the type-B correction and type-C correction of Kastenholz *et al*[79]. Type-C correction is due to an improper summation scheme of the solvent polarization due to the periodicity.

The comparison between the radial distribution functions obtained with 1D IET and 3D MDFT around a sodium cation solute is shown in figure 5. Again, the agreement is almost perfect with a slight overestimation of the second pick of the radial distribution function between  $\text{Na}^+$  and  $\text{Cl}^-$ . Regarding the energetics, the solvation free energy of the sodium cation predicted by MDFT is  $-390.14 \text{ kJ} \cdot \text{mol}^{-1}$  in fairly good agreement with the value of  $-390.37 \text{ kJ} \cdot \text{mol}^{-1}$  predicted using 1D-IET. When the solvent is represented explicitly, the ion-ion radial distribution functions are more structured, exhibiting several

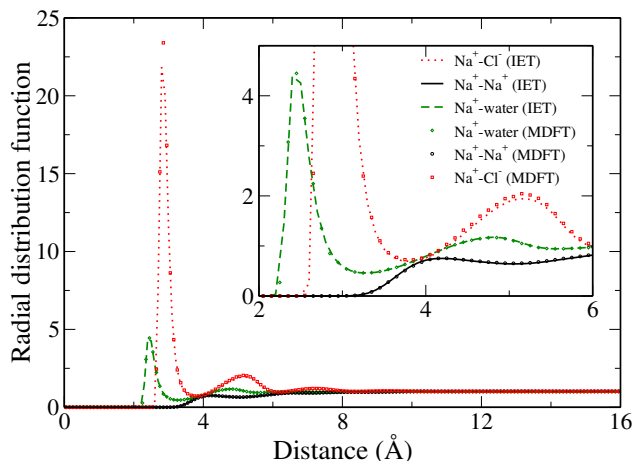


Figure 5. Radial distributions of aqueous NaCl solution around a  $\text{Na}^+$  cation computed using IET (lines) and MDFT (symbols)

maxima, whereas the primitive-like model shows only a single maximum. Moreover the first peak of the sodium-chloride radial distribution function is roughly 10 times higher in the 3 component mixture than in the primitive model. The central cation is immediately surrounded by water molecules which is followed by a shell of counterions. It is worth noting that the sodium cation, despite having the smaller LJ radius, is expelled quite far from the central cation. This contrasts with the primitive-like solvent, where the closest contact was between sodium ions. Clearly, the two solvent descriptions provide two very different pictures of the solvation properties, even for a simple spherical cation.

Again, the primary focus of the present work is to study 3D-shaped solutes. Figure 6 presents density slices in the plane of the NMA molecule. When focusing on the ions, it is evident that the solvation differs significantly from the primitive-like model. For instance, the volume from which the sodium ion is expelled exhibits a "bump" in the vicinity of the hydrogen atom, which was not present in the primitive-like model. Both ion densities show oscillations, indicating the presence of several solvation shells, similar to what was observed in the comparison of the radial distribution function around the sodium cation.

The charge density around the NMA molecule, defined here as the difference between the sodium density and the chloride density for consistency with the primitive like model, exhibits a rather complex structure. There is an excess of positive charge close to the oxygen atom and an excess of negative charge close to the nitrogen atom, which is expected from the electrostatic interactions. However, the successive layers of positive and negative charges

result from the interplay between the three species and the external potential, making their a priori prediction challenging. It is also noteworthy that the present approach properly captures the water structure as evidenced by the density plot in figure 6. On this plot, the polarisation which is defined as

$$\mathbf{P}(\mathbf{r}) = \int \rho_w(\mathbf{r}, \Omega) \Omega d\Omega \quad (21)$$

is represented by arrows. Note that the quantity defined in equation 21 is dimensionless and should be multiplied by  $\mu$ , the dipole of a water molecule, to recover the dipolar polarization. For clarity, the preferential orientations are only represented when  $\|\mathbf{P}(\mathbf{r})\| > \epsilon$ . Here, we arbitrarily choose  $\epsilon$  to be one-tenth of the maximum value of  $\|\mathbf{P}\|$ . There are 3 regions of high water density around the NMA molecule, that are found where hydrogen bonding sites with water are expected. The first one is near the amide hydrogen, with a marked preferential orientation pointing outward the solute. This indicates a strong interaction of water molecules with the oxygen pointing towards the N-H bond. The other two high-density regions are the two lobes close to the oxygen of the NMA molecule, here the water molecules are preferentially oriented with their hydrogen atoms pointing towards the oxygen of NMA.

### C. Conclusions

In this paper, we presented a generalisation of molecular density functional theory (MDFT) to mixtures of solvents, with a focus on the modelling of aqueous electrolytes. While the theoretical extension of MDFT to mixtures is relatively straightforward, its numerical implementation proved to be more subtle. Specifically, it was necessary to modify the relationship between the minimisation variables and the solvent density to ensure that electroneutrality is maintained throughout the minimisation process.

The simplest model of an electrolytic solution is the primitive model. We developed a functional for a similar model consisting of two oppositely charged Lennard-Jones spheres immersed in a dielectric continuum. Since the ions are spherical particles, they are represented by a density  $n_{\pm}(\mathbf{r})$  that does not depend on orientation.

We validated the proposed methodology and its numerical implementation by computing the solvation properties around a  $\text{Na}^+$  and a  $\text{Cl}^-$  solute in a 1M NaCl primitive model solution. Results were compared to predictions obtained using integral equation theories

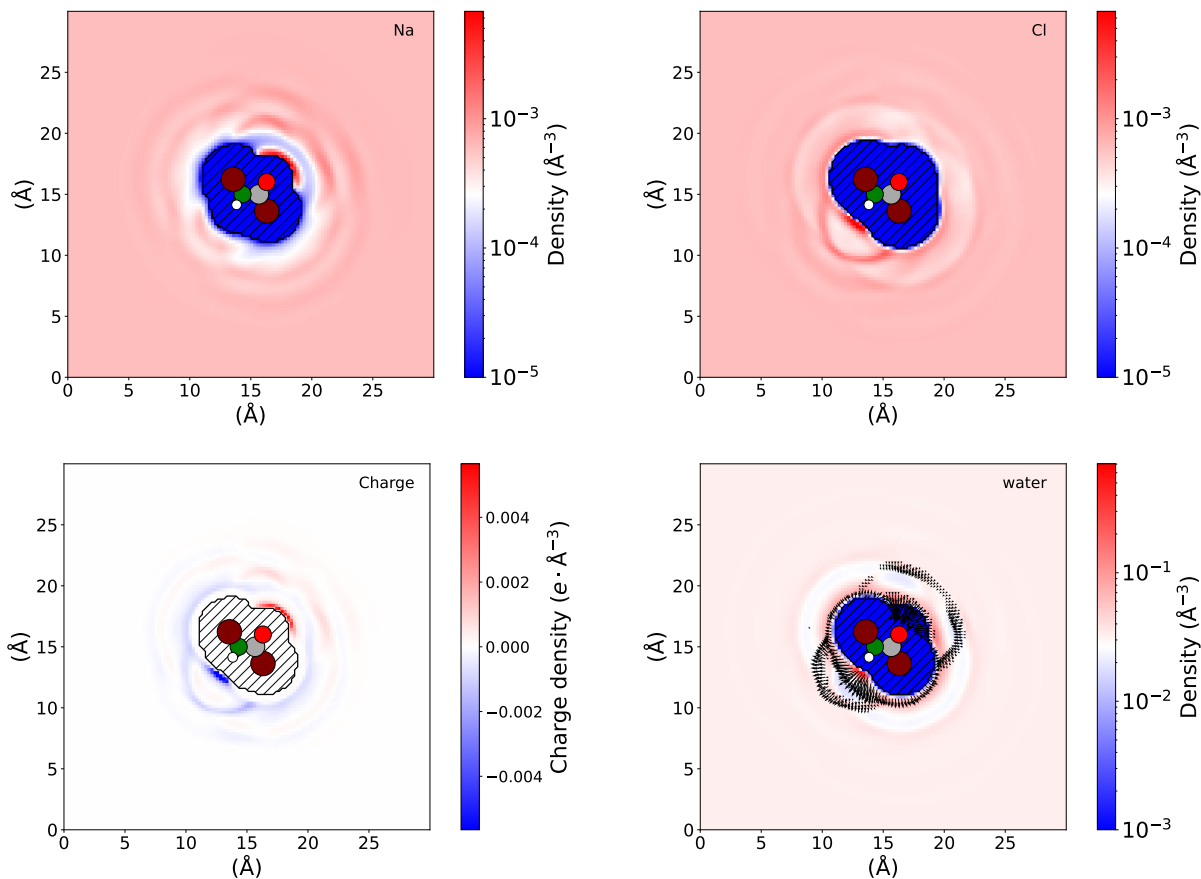


Figure 6. Slices of density in the plane of the NMA molecule. The top panels display the sodium density (left) and the chloride density (right). The bottom panels show the charge density (left), defined as the difference between the sodium density and the chloride density. The bottom right panel display the water density. The arrows represents the water polarisation as defined in equation 21.

for the same system. We observe nearly perfect agreement in both the structure and the solvation free energy. The strength of the present implementation, as compared to integral equation theory, lies in its ability to model tridimensional solutes. For instance, we were able to capture in details the solvation structure of  $\text{Na}^+$  and  $\text{Cl}^-$  around a N-methylacetamide molecule.

In the primitive model, where the electrostatic interactions are screened by a factor 78, the solvation structure is essentially controlled by the finite size interaction, causing the molecule to be unrealistically surrounded by sodium cations. Moreover, there is no structuring beyond the first solvation shell. This limitation of the primitive model highlights

the need for a more refined model of electrolytic solution. Consequently, we adopted a more realistic three-components model for aqueous NaCl at 1M where ions are still represented as oppositely charged spheres but water is now described explicitly using the SPC/E water model.

This more advanced description requires knowledge of 6 independent solvent-solvent direct correlation functions, among which those involving water have an angular dependency. Again, we start by comparing the solvation properties around a  $\text{Na}^+$  cation predicted by MDFT and by IET. The agreement between MDFT and IET is excellent for both structure and free energy. The solvation structure is more complex than in the primitive model case. For instance, the sodium-chloride radial distribution function presents a marked peak corresponding to the first solvation shell. All radial distribution functions exhibit oscillations revealing the presence of several solvation shells and long-range ordering. The NMA molecule also presents a more intricate solvation structure when water is explicitly included, as evidenced by the oscillations in both water and ion densities and the non trivial orientational ordering of the water molecules.

This paper establishes the validity of the functional approach to model molecular electrolytes. The quality of the predictions of the presented HNC functional must be assessed in the future by thorough comparison with explicit simulations and experiments. It might be necessary to introduce bridge functional, specifically designed for electrolytes, to complement the HNC functional. Nevertheless, we believe that MDFT's ability to accurately describe electrolytic solution at a reasonable computational cost will make it a valuable tool to address a wide range of systems in which ions play a key role, such as electrochemical devices and biological systems.

- 
- [1] J. M. Broering and A. S. Bommarius, Evaluation of Hofmeister Effects on the Kinetic Stability of Proteins, *The Journal of Physical Chemistry B* **109**, 20612 (2005).
  - [2] A. C. Dumetz, A. M. Snellinger-O'Brien, E. W. Kaler, and A. M. Lenhoff, Patterns of protein-protein interactions in salt solutions and implications for protein crystallization, *Protein Science* **16**, 1867 (2007).
  - [3] R. Friedman, E. Nachliel, and M. Gutman, Molecular Dynamics of a Protein Surface : Ion-

- Residues Interactions, *Biophysical Journal* **89**, 768 (2005).
- [4] J. Xue, P. Wang, X. Li, R. Tan, and W. Zong, Transformation characteristics of A-DNA in salt solution revealed through molecular dynamics simulations, *Biophysical Chemistry* **288**, 106845 (2022).
  - [5] C. Merlet, B. Rotenberg, P. A. Madden, P.-L. Taberna, P. Simon, Y. Gogotsi, and M. Salanne, On the molecular origin of supercapacitance in nanoporous carbon electrodes, *Nature Materials* **11**, 306 (2012).
  - [6] C. Péan, C. Merlet, B. Rotenberg, P. A. Madden, P.-L. Taberna, B. Daffos, M. Salanne, and P. Simon, On the Dynamics of Charging in Nanoporous Carbon-Based Supercapacitors, *ACS Nano* **8**, 1576 (2014).
  - [7] M. Salanne, B. Rotenberg, K. Naoi, K. Kaneko, P. Taberna, C. P. Grey, B. Dunn, and P. Simon, Efficient storage mechanisms for building better supercapacitors, *Nature Energy* **1**, 16070 (2016).
  - [8] A. A. Kornyshev, Double-layer in ionic liquids : paradigm change?, *The Journal of Physical Chemistry B* **111**, 5545 (2007).
  - [9] F. Fogolari, A. Brigo, and H. Molinari, The Poisson-Boltzmann equation for biomolecular electrostatics : a tool for structural biology, *Journal of Molecular Recognition* **15**, 377 (2002).
  - [10] K. L. Baran, M. S. Chimenti, J. L. Schlessman, C. A. Fitch, K. J. Herbst, and B. E. Garcia-Moreno, Electrostatic Effects in a Network of Polar and Ionizable Groups in Staphylococcal Nuclease, *Journal of Molecular Biology* **379**, 1045 (2008).
  - [11] M. L. Connolly, Computation of molecular volume, *Journal of the American Chemical Society* **107**, 1118 (1985).
  - [12] M. Nina, W. Im, and B. Roux, Optimized atomic radii for protein continuum electrostatics solvation forces, *Biophysical Chemistry* **78**, 89 (1999).
  - [13] S. Gavryushov, Electrostatics of B-DNA in NaCl and CaCl<sub>2</sub> Solutions : Ion Size, Interionic Correlation, and Solvent Dielectric Saturation Effects, *The Journal of Physical Chemistry B* **112**, 8955 (2008).
  - [14] P. Grochowski and J. Trylska, Continuum molecular electrostatics, salt effects, and counterion binding-A review of the Poisson-Boltzmann theory and its modifications, *Biopolymers* **89**, 93 (2008).
  - [15] P. Ren, J. Chun, D. G. Thomas, M. J. Schnieders, M. Marucho, J. Zhang, and N. A. Baker,

- Biomolecular electrostatics and solvation : a computational perspective, *Quarterly Reviews of Biophysics* **45**, 427 (2012).
- [16] D. Chandler and H. C. Andersen, Optimized Cluster Expansions for Classical Fluids. II. Theory of Molecular Liquids, *The Journal of Chemical Physics* **57**, 1930 (1972).
  - [17] F. Hirata and P. J. Rossky, An extended rism equation for molecular polar fluids, *Chemical Physics Letters* **83**, 329 (1981).
  - [18] D. Beglov and B. Roux, An Integral Equation To Describe the Solvation of Polar Molecules in Liquid Water, *The Journal of Physical Chemistry B* **101**, 7821 (1997).
  - [19] A. Kovalenko and F. Hirata, *Chemical Physics Letters* **290**, 237 (1998).
  - [20] A. Kovalenko and F. Hirata, Potentials of mean force of simple ions in ambient aqueous solution. I. Three-dimensional reference interaction site model approach, *The Journal of Chemical Physics* **112**, 10391 (2000).
  - [21] T. Kloss, J. Heil, and S. M. Kast, Quantum Chemistry in Solution by Combining 3D Integral Equation Theory with a Cluster Embedding Approach, *The Journal of Physical Chemistry B* **112**, 4337 (2008).
  - [22] F. Hoffgaard, J. Heil, and S. M. Kast, Three-Dimensional RISM Integral Equation Theory for Polarizable Solute Models, *Journal of Chemical Theory and Computation* **9**, 4718 (2013).
  - [23] T. Imai, R. Hiraoka, A. Kovalenko, and F. Hirata, Water Molecules in a Protein Cavity Detected by a Statistical-Mechanical Theory, *Journal of the American Chemical Society* **127**, 15334 (2005).
  - [24] N. Yoshida, T. Imai, S. Phongphanphanee, A. Kovalenko, and F. Hirata, Molecular Recognition in Biomolecules Studied by Statistical-Mechanical Integral-Equation Theory of Liquids, *The Journal of Physical Chemistry B* **113**, 873 (2009).
  - [25] M. Sugita, M. Hamano, K. Kasahara, T. Kikuchi, and F. Hirata, New Protocol for Predicting the Ligand-Binding Site and Mode Based on the 3D-RISM/KH Theory, *Journal of Chemical Theory and Computation* **16**, 2864 (2020).
  - [26] K. Osaki, T. Ekimoto, T. Yamane, and M. Ikeguchi, 3D-RISM-AI : A Machine Learning Approach to Predict Protein-Ligand Binding Affinity Using 3D-RISM, *The Journal of Physical Chemistry B* **126**, 6148 (2022).
  - [27] Y. Maruyama, N. Yoshida, and F. Hirata, Revisiting the Salt-Induced Conformational Change of DNA with 3D-RISM Theory, *The Journal of Physical Chemistry B* **114**, 6464 (2010).

- [28] G. M. Giambaşu, M. K. Gebala, M. T. Panteva, T. Luchko, D. A. Case, and D. M. York, Competitive interaction of monovalent cations with DNA from 3D-RISM, *Nucleic Acids Research* **43**, 8405 (2015).
- [29] F. Hirata, *Molecular Theory of Solvation* (2003).
- [30] N. D. Mermin, Thermal Properties of the Inhomogeneous Electron Gas, *Physical Review* **137**, A1441 (1965).
- [31] R. Evans, The nature of the liquid-vapour interface and other topics in the statistical mechanics of non-uniform, classical fluids, *Advances in Physics* **28**, 143 (1979).
- [32] R. D. Groot, Density-functional theory for inhomogeneous electrolytes, *Physical Review A* **37**, 3456 (1988).
- [33] L. Mier-y Teran, S. H. Suh, H. S. White, and H. T. Davis, A nonlocal free-energy density-functional approximation for the electrical double layer, *The Journal of Chemical Physics* **92**, 5087 (1990).
- [34] E. Kierlik and M. L. Rosinberg, Density-functional theory for inhomogeneous fluids : Adsorption of binary mixtures, *Physical Review A* **44**, 5025 (1991).
- [35] Y. Rosenfeld, Free-energy model for the inhomogeneous hard-sphere fluid mixture and density-functional theory of freezing, *Physical Review Letters* **63**, 980 (1989).
- [36] R. Roth, R. Evans, A. Lang, and G. Kahl, Fundamental measure theory for hard-sphere mixtures revisited : the White Bear version, *Journal of Physics : Condensed Matter* **14**, 12063 (2002).
- [37] H. Hansen-Goos and R. Roth, Density functional theory for hard-sphere mixtures : the White Bear version mark II, *Journal of Physics : Condensed Matter* **18**, 8413 (2006).
- [38] J. Forsman, C. E. Woodward, and R. Szparaga, Classical Density Functional Theory of Ionic Solutions, in *Computational Electrostatics for Biological Applications : Geometric and Numerical Approaches to the Description of Electrostatic Interaction Between Macromolecules*, edited by W. Rocchia and M. Spagnuolo (Cham, 2015) pp. 17–38.
- [39] C. Azuara, H. Orland, M. Bon, P. Koehl, and M. Delarue, Incorporating Dipolar Solvents with Variable Density in Poisson-Boltzmann Electrostatics, *Biophysical Journal* **95**, 5587 (2008).
- [40] A. Härtel, M. Janssen, S. Samin, and R. v. Roij, Fundamental measure theory for the electric double layer : implications for blue-energy harvesting and water desalination, *Journal of Physics : Condensed Matter* **27**, 194129 (2015).



- [41] P. Cats, R. S. Sitlapersad, W. K. den Otter, A. R. Thornton, and R. van Roij, Capacitance and Structure of Electric Double Layers : Comparing Brownian Dynamics and Classical Density Functional Theory, *Journal of Solution Chemistry* **51**, 296 (2022).
- [42] Y. Levin, Electrostatic correlations : from plasma to biology, *Reports on Progress in Physics* **65**, 1577 (2002).
- [43] R. D. Groot, Ion condensation on solid particles : Theory and simulations, *The Journal of Chemical Physics* **95**, 9191 (1991).
- [44] R. Roth and D. Gillespie, Shells of charge : a density functional theory for charged hard spheres, *Journal of Physics : Condensed Matter* **28**, 244006 (2016).
- [45] S.-C. Lin, G. Martius, and M. Oettel, Analytical classical density functionals from an equation learning network, *The Journal of Chemical Physics* **152**, 021102 (2020).
- [46] P. Cats, S. Kuipers, S. de Wind, R. van Damme, G. M. Coli, M. Dijkstra, and R. van Roij, *APL Materials* **9**, 031109 (2021).
- [47] F. Sammüller, S. Hermann, D. de las Heras, and M. Schmidt, Neural functional theory for inhomogeneous fluids : Fundamentals and applications, *Proceedings of the National Academy of Sciences* **120**, e2312484120 (2023).
- [48] A. T. Bui and S. J. Cox, Learning Classical Density Functionals for Ionic Fluids, *Physical Review Letters* **134**, 148001 (2025).
- [49] G. Yang and L. Liu, A systematic comparison of different approaches of density functional theory for the study of electrical double layers, *The Journal of Chemical Physics* **142**, 194110 (2015).
- [50] A. Oleksy and J.-P. Hansen, Towards a microscopic theory of wetting by ionic solutions. I. Surface properties of the semi-primitive model, *Molecular Physics* **104**, 2871 (2006).
- [51] D.-e. Jiang, Z. Jin, D. Henderson, and J. Wu, Solvent Effect on the Pore-Size Dependence of an Organic Electrolyte Supercapacitor, *The Journal of Physical Chemistry Letters* **3**, 1727 (2012).
- [52] D.-e. Jiang and J. Wu, Microscopic Insights into the Electrochemical Behavior of Nonaqueous Electrolytes in Electric Double-Layer Capacitors, *The Journal of Physical Chemistry Letters* , 1260 (2013).
- [53] C. Lian, C. Zhan, D.-e. Jiang, H. Liu, and J. Wu, Capacitive Energy Extraction by Few-Layer Graphene Electrodes, *The Journal of Physical Chemistry C* **121**, 14010 (2017).

- [54] T. Biben, J. P. Hansen, and Y. Rosenfeld, Generic density functional for electric double layers in a molecular solvent, *Physical Review E* **57**, R3727 (1998).
- [55] A. Oleksy and J.-P. Hansen, Wetting of a solid substrate by a "civilized" model of ionic solutions, *The Journal of Chemical Physics* **132**, 204702 (2010).
- [56] A. Oleksy and J.-P. Hansen, Wetting and drying scenarios of ionic solutions, *Molecular Physics* **109**, 1275 (2011).
- [57] G. Jeanmairet, M. Levesque, R. Vuilleumier, and D. Borgis, Molecular Density Functional Theory of Water, *The Journal of Physical Chemistry Letters* **4**, 619 (2013).
- [58] M. Beicastro, T. Marino, T. Mineva, N. Russo, E. Sicilia, and M. Toscano, Density Functional Theory as a Tool for the Prediction of the Properties in Molecules with Biological and Pharmacological Significance, in *Theoretical and Computational Chemistry*, Recent Developments and Applications of Modern Density Functional Theory, Vol. 4, edited by J. M. Seminario (1996) pp. 743–772.
- [59] W. S. B. Dwandaru and M. Schmidt, Variational principle of classical density functional theory via Levy’s constrained search method, *Physical Review E* **83**, 061133 (2011).
- [60] G. Jeanmairet, M. Labat, and E. Giner, A variational formulation of the free energy of mixed quantum-classical systems : coupling classical and electronic density functional theories (2025), <http://arxiv.org/abs/2411.11821>.
- [61] J.-P. Hansen and I. McDonald, *Theory of Simple Liquids, Third Edition*, 3rd ed. (2006).
- [62] G. Jeanmairet, M. Levesque, and D. Borgis, Tackling Solvent Effects by Coupling Electronic and Molecular Density Functional Theory, *Journal of Chemical Theory and Computation* **16**, 7123 (2020).
- [63] M. Labat, E. Giner, and G. Jeanmairet, Coupling molecular density functional theory with converged selected configuration interaction methods to study excited states in aqueous solution, *The Journal of Chemical Physics* **161**, 014113 (2024).
- [64] M. Labat, G. Jeanmairet, and E. Giner, Prediction of the aqueous redox properties of functionalized quinones using a new QM/MM variational formulation (2025).
- [65] M. Levesque, V. Marry, B. Rotenberg, G. Jeanmairet, R. Vuilleumier, and D. Borgis, Solvation of complex surfaces via molecular density functional theory, *The Journal of Chemical Physics* **137**, 224107 (2012).
- [66] G. Jeanmairet, M. Levesque, V. Sergiievskiy, and D. Borgis, Molecular density functional

- theory for water with liquid-gas coexistence and correct pressure, *The Journal of Chemical Physics* **142**, 154112 (2015).
- [67] D. Borgis, S. Luukkonen, L. Belloni, and G. Jeanmairet, Simple Parameter-Free Bridge Functionals for Molecular Density Functional Theory. Application to Hydrophobic Solvation, *The Journal of Physical Chemistry B* **124**, 6885 (2020).
- [68] D. Borgis, S. Luukkonen, L. Belloni, and G. Jeanmairet, Accurate prediction of hydration free energies and solvation structures using molecular density functional theory with a simple bridge functional, *The Journal of Chemical Physics* **155**, 024117 (2021).
- [69] T.-Y. Hsu and G. Jeanmairet, Assessing the correctness of pressure correction to solvation theories in the study of electron transfer reactions, *The Journal of Chemical Physics* **154**, 131102 (2021).
- [70] L. Belloni and I. Chikina, Efficient full Newton-Raphson technique for the solution of molecular integral equations - example of the SPC/E water-like system, *Molecular Physics* **112**, 1246 (2014).
- [71] L. Belloni, Exact molecular direct, cavity, and bridge functions in water system, *The Journal of Chemical Physics* **147**, 164121 (2017).
- [72] L. Blum, Invariant Expansion. II. The Ornstein-Zernike Equation for Nonspherical Molecules and an Extended Solution to the Mean Spherical Model, *The Journal of Chemical Physics* **57**, 1862 (1972).
- [73] L. Ding, M. Levesque, D. Borgis, and L. Belloni, Efficient molecular density functional theory using generalized spherical harmonics expansions, *The Journal of Chemical Physics* **147**, 094107 (2017).
- [74] L. Blum and A. J. Torruella, Invariant Expansion for Two-Body Correlations : Thermodynamic Functions, Scattering, and the Ornstein-Zernike Equation, *The Journal of Chemical Physics* **56**, 303 (1972).
- [75] L. Blum, Invariant expansion III : The general solution of the mean spherical model for neutral spheres with electrostatic interactions, *The Journal of Chemical Physics* **58**, 3295 (1973).
- [76] M. Frigo and S. Johnson, The Design and Implementation of FFTW3, *Proceedings of the IEEE* **93**, 216 (2005).
- [77] C. Zhu, R. H. Byrd, P. Lu, and J. Nocedal, Algorithm 778 : L-BFGS-B : Fortran subroutines for large-scale bound-constrained optimization, *ACM Transactions on Mathematical Software*

- 23**, 550 (1997).
- [78] P. H. Fries and G. N. Patey, The solution of the hypernetted-chain approximation for fluids of nonspherical particles. A general method with application to dipolar hard spheres, *The Journal of Chemical Physics* **82**, 429 (1985).
- [79] M. A. Kastholz and P. H. Hünenberger, Computation of methodology-independent ionic solvation free energies from molecular simulations. II. The hydration free energy of the sodium cation, *The Journal of Chemical Physics* **124**, 224501 (2006).